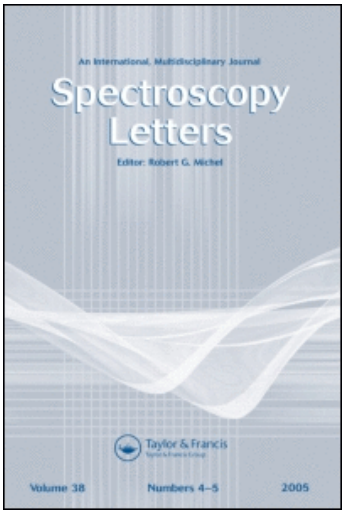

Spectroscopy Letters
Publication details, including instructions for authors and subscription information:
http://www.informaworld.com/smpp/title~content=t713597299

Lanthanide-Containing 2,2'-Bipyridine Bridged Urea Cross-Linked Polysilsesquioxanes

Sónia S. Nobre[ab]; Rute A. S. Ferreira[a]; Xavier Cattoën[b]; Sofia Benyahya[b]; Marc Taillefer[b]; Verónica de Zea Bermudez[c]; Michel Wong Chi Man[b]; Luis D. Carlos[a]
[a] Department of Physics, University of Aveiro, Aveiro, Portugal [b] Institut Charles Gerhardt Montpellier, Ecole Nationale Supérieure de Chimie de Montpellier UMR 5253 CNRS-UMII-ENSCM-UMI, France [c] Department of Chemistry, University of Trás-os-Montes e Alto, Douro, Vila Real, Portugal

Online publication date: 30 July 2010

To cite this Article Nobre, Sónia S. , Ferreira, Rute A. S. , Cattoën, Xavier , Benyahya, Sofia , Taillefer, Marc , Bermudez, Verónica de Zea , Chi Man, Michel Wong and Carlos, Luis D.(2010) 'Lanthanide-Containing 2,2'-Bipyridine Bridged Urea Cross-Linked Polysilsesquioxanes', Spectroscopy Letters, 43: 5, 321 — 332
To link to this Article: DOI: 10.1080/00387010.2010.486712
URL: http://dx.doi.org/10.1080/00387010.2010.486712

Spectroscopy Letters, 43:321–332, 2010

ISSN: 0038-7010 print/1532-2289 online
DOI: 10.1080/00387010.2010.486712

Taylor & Francis
Taylor & Francis Group

Lanthanide-Containing 2,2′-Bipyridine Bridged Urea Cross-Linked Polysilsesquioxanes

Sónia S. Nobre[1,2], Rute A. S. Ferreira[1], Xavier Cattoën[2], Sofia Benyahya[2], Marc Taillefer[2], Verónica de Zea Bermudez[3], Michel Wong Chi Man[2], and Luis D. Carlos[1]

[1]Department of Physics, University of Aveiro, Aveiro, Portugal
[2]Institut Charles Gerhardt Montpellier, Ecole Nationale Supérieure de Chimie de Montpellier UMR 5253 CNRS–UMII–ENSCM–UMI, France
[3]Department of Chemistry, University of Trás-os-Montes e Alto, Douro, Vila Real, Portugal

ABSTRACT Urea-based bis-silylated 2,2′–Bipyridine (bpy) organic–inorganic hybrids incorporating different lanthanide (Ln^{3+}) ions (Eu^{3+}, Gd^{3+}, Tb^{3+} or Eu^{3+}/Tb^{3+}) were obtained by the sol–gel process. The structure and the emission characteristics of the hybrids were ascertained using X-ray diffraction, nuclear magnetic resonance, Fourier transform infrared spectroscopy, photoluminescence, and quantum yield measurements. The hybrids feature both the emission of the host and the Eu^{3+} and/or Tb^{3+} transitions allowing a fine-tuning of the color from the blue to the red, orange, or green spectral regions. Bpy-to-Ln^{3+} and Tb^{3+}-to-Eu^{3+} energy transfer mechanisms are demonstrated and the hybrids present slightly distinct Ln^{3+} coordination spheres due to the different bpy/Ln^{3+} ratios.

KEYWORDS 2,2′-Bipyridine, bridged polysilsesquioxanes, lanthanides, photoluminescence, sol-gel, urea

INTRODUCTION

The interest in lanthanide-containing organic–inorganic hybrids has grown considerably during the last decade with the concomitant fabrication of materials with tunable attributes offering modulated properties. The potential of these materials relies on the exploitation of the synergy between the intrinsic characteristics of sol–gel derived hosts (highly controlled purity, versatile shaping and patterning, excellent optical quality, easy control of the refractive index, photosensitivity, encapsulation of large amounts of isolated emitting centers by the host cage) and the luminescence features of trivalent lanthanide ions (Ln^{3+}) (high luminescence quantum yield, narrow bandwidth, long-lived emission, large Stokes shifts, ligand-dependent luminescence sensitization).[1–3]

2,2′-bipyridine (bpy) is one of the most commonly used ligands in the design of highly luminescent Ln^{3+}-containing materials because of its intense absorption band in the near-UV and its ability to efficiently transfer energy onto the Ln^{3+} excited states (antenna effect).[4,5] Since the pioneering work of Franville et al. [6] on pyridyl-amide based hybrids, a handful of studies were reported on bpy-based Ln^{3+}-containing materials either obtained by

Received 13 October 2009; accepted 29 October 2009.

Address correspondence to Luis D. Carlos, Department of Physics, CICECO, University of Aveiro, 3810-193 Aveiro, Portugal. E-mail: lcarlos@ua.pt

co-gelification with a silica source (e.g., tetramethylorthosilicate (TMOS) or tetraethylorthosilicate (TEOS)),[7–9] or directly from a single precursor.[10] The main advantages of the latter method are: i) materials with an homogeneous distribution of organics within the silica network are obtained; ii) a controlled and higher loading of organics and Ln^{3+} ions can be incorporated; iii) self-structuring may be envisaged in the presence of self-assembling groups in the organic fragments.[11] Recently, a bis(4,4′-diurea-2,2′-bpy) silylated derivative (incorporating Eu^{3+} and Tb^{3+} ions) was used simultaneously for catalytic[12] and luminescence[10] applications.

In this work we present new insights into the photoluminescence of these urea/bpy-based hybrids incorporating Eu^{3+}, Gd^{3+}, and/or Tb^{3+} ions. Moreover, we demonstrate for the first time the key role played by the light emitted by the hybrid host in the luminescence of the corresponding Ln^{3+}-based hybrids. We also report that the fine tuning of the emission color of the materials along the *Commission Internationale d'Éclairage* (CIE)-1931 chromaticity diagram can be achieved through the variation of the mixture of lanthanide species used and the excitation wavelength.

EXPERIMENTAL

Synthesis of the Hybrid Materials

The synthesis of the bpy-based precursor (**P**) (Scheme 1) was described in detail elsewhere.[12] The preparation of the Ln^{3+}-doped hybrids (Ln = Eu, Eu, Gd, Tb or 1:1 mixture of Eu and Tb) consisted of stirring, at 45°C for 5 minutes, an homogeneous mixture of **P**, water (H_2O), ammonium fluoride (NH_4F) and lanthanide chloride hexahydrate ($LnCl_3 \cdot 6H_2O$),

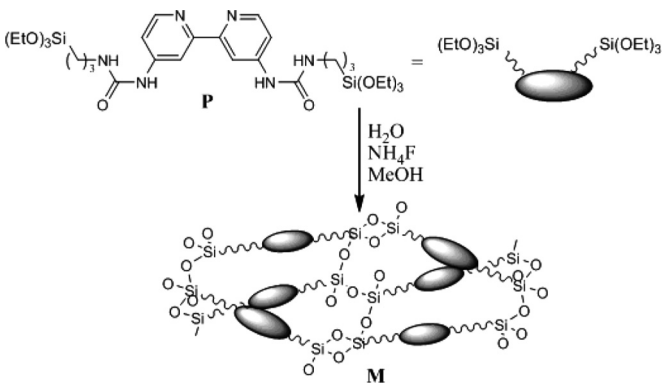

SCHEME 1 **Schematic representation of the M synthesis.**

(molar ratio **P**/($LnCl_3 \cdot 6H_2O$)/H_2O/NH_4F:1/0.33/30/0.01) at 0.1 mol · L^{-1} in methanol (freshly dried over magnesium and distilled). After 3 hours, the resulting gel was aged for 3 days at room temperature to yield a white monolith. The Ln^{3+}-containing hybrids were designated by **M-Ln** (Ln = Eu, Gd, and Tb) or **M-EuTb** (Eu/Tb mixture). The synthesis of the non-doped hybrid, abbreviated as **M**, was performed in a similar fashion. Elemental analyses for the Si, N and Ln atoms were performed for all the hybrids and the obtained values, in % (w/w), were: **M** (Si, 8.54; N, 16.27), **M-Eu** (Si, 8.29; N, 14.10; Eu 4.98), **M-Gd** (Si, 7.27; N, 12.61; Gd, 7.44), **M-Tb** (Si, 8.22; N, 13.29; Tb, 6.34) and **M-EuTb** (Si, 6.10; N, 13.70; Eu, 2.68; Tb, 3.37). The calculated bpy/Ln ratios were 5.1, 3.2, 4.0 and 4.2, for **M-Eu**, **M-Gd**, **M-Tb** and **M-EuTb**, respectively. Previously, Li et al. made the assumption that a bpy/Ln = 2/1 ratio was formed in similar materials.[10] Nevertheless, in the **M-Ln** hybrids reported here the formation of a 3/1 ratio cannot be discarded. In any case, it appears that free and Ln^{3+}-complexed ligands co-exist in all the samples.

Experimental Techniques

X-Ray Diffraction (XRD)

XRD patterns were recorded using a Philips X'Pert MPD powder X-ray diffractometer. The samples were exposed to the CuK_α radiation (1.54 Å) in a 2θ range between 1.00 and 60.00° with a step of 0.05 and time-acquisition per step of 40 s.

Elemental Analysis

The Eu and Si content were obtained by ICP-OES (Inductively Coupled Plasma Optical Emission Spectroscopy) analysis on a Horiba Jobin-Yvon Activa-M instrument with a glass concentric nebulizer. For Eu content determination the samples were first digested under microwaves with 6 mL of HCl, 2 mL of HNO_3 and 1 mL of HF at 150°C and then dried. The F^- ion was removed by two successive additions of 5 mL of HCl after evaporation. The solution was recovered in 10 mL of HNO_3 20% and diluted. For Si content determination the samples were first digested under microwaves with 6 mL of HCl, 2 mL of HNO_3 and 1 mL of HF and then diluted. The experimental error was within 10%. Elemental analyses for C, H, and N were performed with a CHNS-932

Elemental analyzer with standard combustion conditions and handling of the samples at air.

Fourier Transform Infrared (FT-IR)

The FT-IR spectra were acquired at room temperature using a Mattson Mod 7000 spectrometer. The spectra were collected in the 4000 to 400 cm^{-1} range by averaging 64 scans at a resolution of 4 cm^{-1}. The solid samples (2 mg) were finely ground, mixed with approximately 175 mg of dried KBr (Merck, spectroscopic grade) and pressed into pellets. Prior to recording the spectra the pellets were stored under vacuum for about 24 hours at approximately 60°C to reduce the levels of adsorbed water.

^{29}Si Magic-Angle Spinning (MAS) Nuclear Magnetic Resonance (NMR) and ^{13}C Cross-Polarization (CP) MAS NMR Spectra

^{13}C, and ^{29}Si solid-state NMR spectra were obtained with a Bruker FT-AM 200 or FT-AM 400 spectrometers using the CP-MAS technique and tetramethylsilane (TMS) as reference for the chemical shifts.

Photoluminescence

Emission and excitation spectra were recorded between 11 K and room temperature with a modular double grating excitation spectrofluorimeter (fitted with a 1200 grooves/mm grating blazed at 330 nm) with a TRIAX 320 emission monochromator (fitted with a 1200 grooves/mm grating blazed at 500 nm), Fluorolog-3, Jobin Yvon-Spex, coupled to a R928 Hamamatsu photomultiplier, using the front face acquisition mode. The excitation source was a 450 W Xe arc lamp. The emission spectra were corrected for detection and optical spectral response of the spectrofluorimeter and the excitation spectra were corrected for the spectral distribution of the lamp intensity using a photodiode reference detector. Time-resolved measurements were carried out with the setup described for the luminescence spectra using a pulsed Xe–Hg lamp (6 μs pulse at half width and 20 to 30 μs tail).

Absolute Emission Quantum Yields

The quantum yields were measured at room temperature using a quantum yield measurement system C9920-02 from Hamamatsu with a 150 W Xenon lamp coupled to a monochromator for wavelength discrimination, an integrating sphere as sample chamber and a multi-channel analyzer for signal detection. Three measurements were made for each sample so that the average value is reported. The method is accurate within 10%.

RESULTS AND DISCUSSION

Structural Description

The XRD patterns of **M** and Ln^{3+}-containing hybrids are shown in Fig. 1 of Supporting Information. The diffractogram of **M** is dominated by a

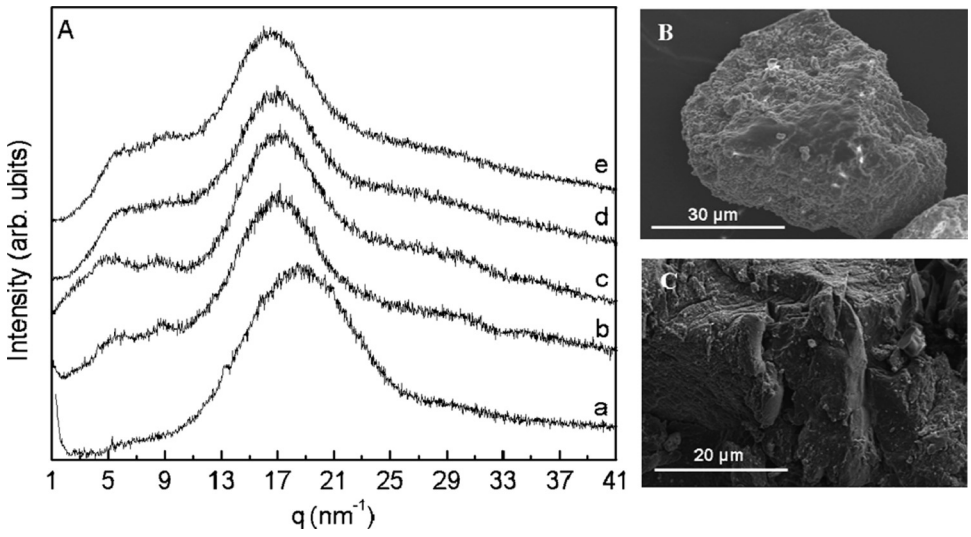

FIGURE 1 (A) XRD patterns of a) M, b) M-Eu, c) M-Tb, d) M-EuTb and e) M-Gd. SEM images of (B) M and (C) M-Eu.

broad band centred at *ca.* 19 nm^{-1} indicative of the amorphous nature of the material. The shift of this band to low q values after the incorporation of the Ln salt (*ca.* 17 nm^{-1}) is believed to be induced by the coordination of Eu^{3+} ions to some bpy molecules with the concomitant increase of the mean distance between the organic moieties.[11] That coordination has been examined in depth by FT-IR and is discussed below.

^{29}Si MAS NMR data were obtained only for **M**, because for the Ln^{3+}-containing hybrids the paramagnetism of the metal ions inhibits such measurements. The spectrum of **M** displays broad signals at −44.9, −57.1 and −67.0 ppm (Fig. 2) ascribed to the $R'Si(OSi)(OH)_2$ (T_1), $R'Si(OSi)_2(OH)$ (T_2) and $R'Si(OSi)_3$ (T_3) silicon environments, respectively. The condensation degree (86%) was calculated using the expression $c = 1/3\ (\%T_1 + 2\%T_2 + 3\%T_3)$. The high degree of condensation is in agreement with the values already reported for organic-inorganic hybrids prepared by fluoride (F^-) ion-catalyzed hydrolysis.[13] It is noteworthy that no Q-type environments are observed, evidencing that the Si-C bonds were not cleaved during the synthesis. This result was confirmed in the ^{13}C NMR spectrum of **M** (Fig. 3), which exhibits a signal at 10 ppm assignable to the propyl carbon atoms directly bonded to the silicon atoms. The ^{13}C CP/MAS NMR spectrum of **M-Eu** resembles closely that of **M** (Fig. 3 of Supporting Information). The resonances match with the corresponding signals of the precursor in solution NMR (dmso-d_6). The absence of signals at 18 and 58 ppm (ethoxyl groups) points out a complete hydrolysis of the Si-OEt groups under the reaction conditions. Due to the larger broadening induced by the higher paramagnetism of Tb^{3+}, the spectra of **M-Tb** and **M-EuTb** could not be recorded.

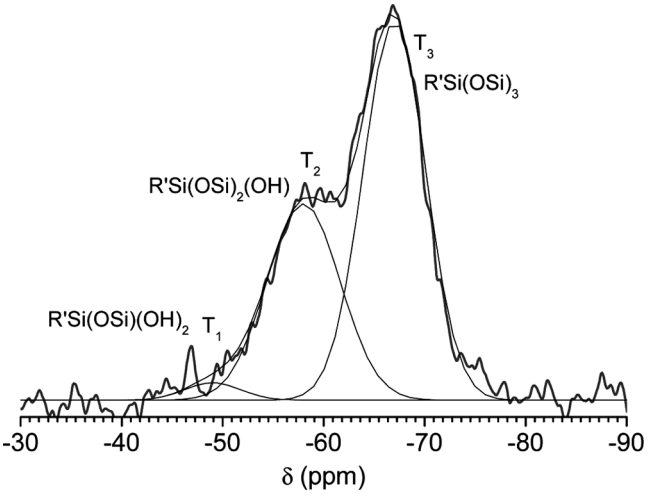

FIGURE 2 **^{29}Si NMR spectrum of M. The solid lines represent the fit using Gaussian functions.**

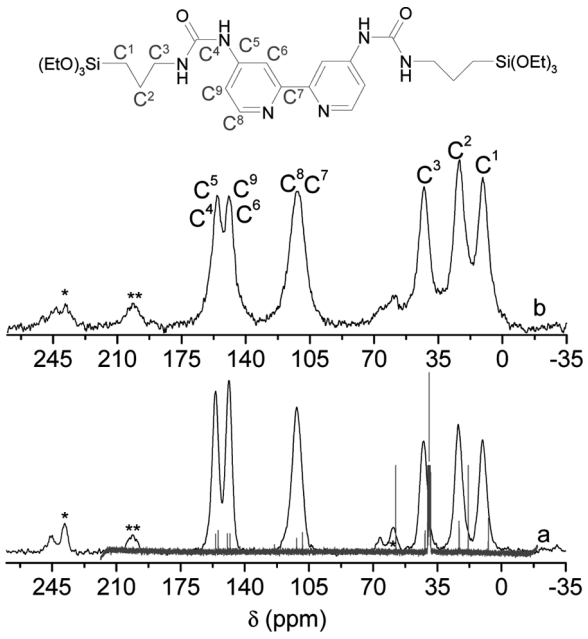

FIGURE 3 **^{13}C CP/MAS NM2R 11spectra of a) M and b) M-Eu acquired in solid state (*black lines*) and (*in solution grey line*). The asterisks correspond to the side spin bands of the peaks at 155.6, 148.6, and 111.7 ppm.**

To add some insights into the composition of the Eu^{3+} coordination sphere, we have recorded the FT-IR spectra of **M**, **M-Eu**, **M-Tb,** and **M-EuTb**. IR spectroscopy is particularly useful to elucidate ligand-Lewis acid interactions in the case of bpy-based complexes, since the vibration modes of this ligand in the free and complexed states have been widely investigated and their attribution is well established.[10,14–20]

We have examined three spectral intervals of the IR spectrum of bpy that are known to be sensitive to coordination effects: (i) 1480–1420 cm^{-1} interval. It is characteristic of ring stretching (ν_{ring}) modes[17,20] (i.e., $\nu_{C=C}$ and/or $\nu_{C=N}$) and, according to some authors,[14,16,19] also CH deformation (δCH) modes. (ii) 1175–945 cm^{-1} interval. While most authors agree that it includes ring breathing modes and coupled ring deformation (δ_{ring}) and δCH modes,[14,16,17,19] some suggest that it also[14,16] or only[20] comprises in-plane δCH ($\delta_{i.p.}$CH) modes. (iii) 850 to 600 cm^{-1} interval. Typically in this region

out-of-plane δCH ($\delta_{o.p.}$CH) modes and in-plane δ_{ring} ($\delta_{i.p.}$ring) modes absorb.[14,16,17,19,20]

Figure 4A reproduces the spectral signature of the four samples under study in the 1480 to 1420 cm^{-1} interval. These spectra demonstrate that the addition of Eu^{3+} and Tb^{3+} ions, alone or mixed, to the **M** framework leads to the emergence of a new feature at 1434 cm^{-1}. Another change resulting from the presence of the Ln^{3+} ions is the shift of the band centered at *ca.* 1467 cm^{-1} to 1471 cm^{-1}. Figure 4B shows that the 996 cm^{-1} mode of free bpy undergoes an upshift to 1003 cm^{-1} upon coordination. Another effect detected in this region is the shift of the intensity maximum at 1026 cm^{-1} to 1032 cm^{-1}. The third region examined, depicted in Fig. 4C, reveals that the addition of the Ln^{3+} salt(s) to the **M** matrix leads to the growth of new features at 778, 734 and 654 cm^{-1}.

Many of the spectral modifications (band shifts and/or emergence of new bands) referred above for the Ln^{3+}-containing hybrids have been reported previously for Ru(II),[17,19] Ir(III),[19] Cr(VI),[20] Mo(VI),[20] W(VI),[20] and Ln-based complexes,[10,14,18] as well as, for intercalation compounds,[15,16] providing evidence that the bpy ligands of **M** framework bond to the Ln^{3+} ions in the doped samples. In all the cases, in spite of the growth of new bands attributed to Ln-bpy complex formation, the bands due to the free ligand do not vanish, indicating that non-coordinated (free) bpy ligands remain in the matrix. This is an expected result, considering the low concentration of guest salts in the xerogel samples.

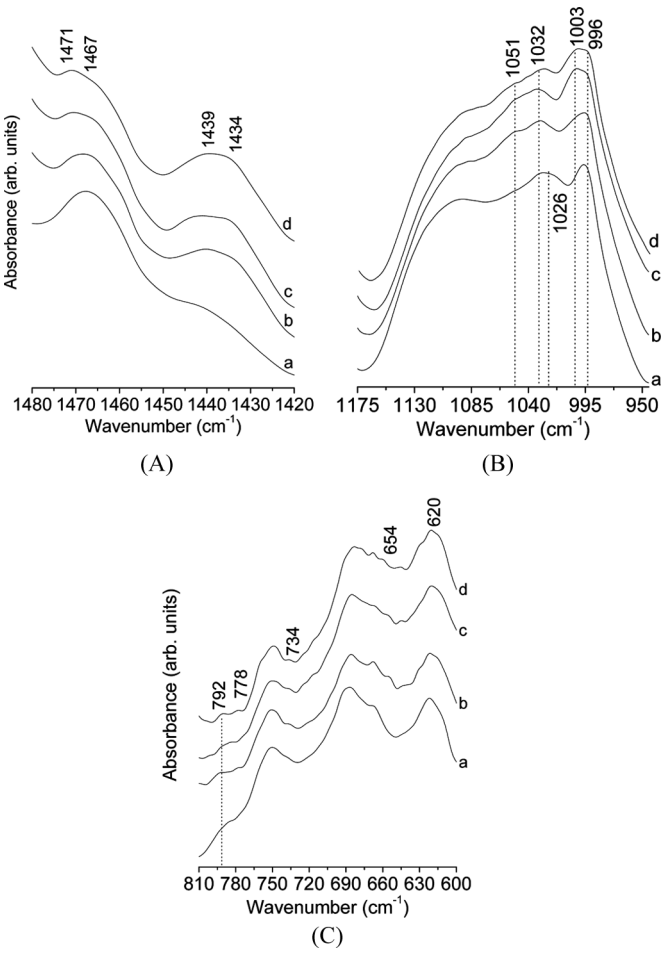

FIGURE 4 **Three mid-FT-IR spectral intervals (A, B and C) of a) M, b) M-Eu, c) M-Tb and d) M-EuTb.**

It is of interest to emphasize that one of the most solid proofs of the formation of the Ln-bpy adduct in the hybrids studied is the emergence of the 1434 cm^{-1} feature in the FT-IR spectra of **M-Eu**, **M-Tb**, and **M-EuTb** (Fig. 4A). It is worth noting that Álvaro et al.[18] and Tsaryuk et al.[14] also detected this feature in the infrared spectra of bpy-based complexes of Eu^{3+}. Finally, a comment is necessary concerning the possibility of bonding of the carbonyl (C=O) oxygen atoms of the urea cross-linkages to the Ln^{3+} ions. Although this hypothesis cannot be discarded, we may speculate simply from the standpoint of steric considerations that the approach of the C=O groups to the emitting centers is rather difficult. Inspection of the "amide I" and "amide II" bands (essentially associated with the C=O stretching and N–H in-plane bending modes, respectively) in the 1800 to 1600 and 1600 to 1500 cm^{-1} band envelopes, respectively, is complex, since both spectral intervals are superimposed with several bpy characteristic ν_{ring} modes.[10,14,16,17,19,20]

Photoluminescence

The hybrids are multi-wavelength emitters under UV excitation. Figure 5 illustrates the emission features of **M-Eu** and **M-Tb** under distinct excitation wavelengths showing a series of peaks, attributed to the Eu^{3+} $^5D_0 \rightarrow {}^7F_{0-4}$ (**M-Eu**) and Tb^{3+} $^5D_4 \rightarrow {}^7F_{6-0}$ (**M-Tb**) transitions, superimposed on a large broad band. Whereas the energy and full width at half maximum (fwhm) of the intra-4f transitions are almost independent of the excitation wavelength, suggesting that the Ln^{3+} ions occupy the same average local environment (see below), the broad band energy and fwhm strongly depend on the excitation

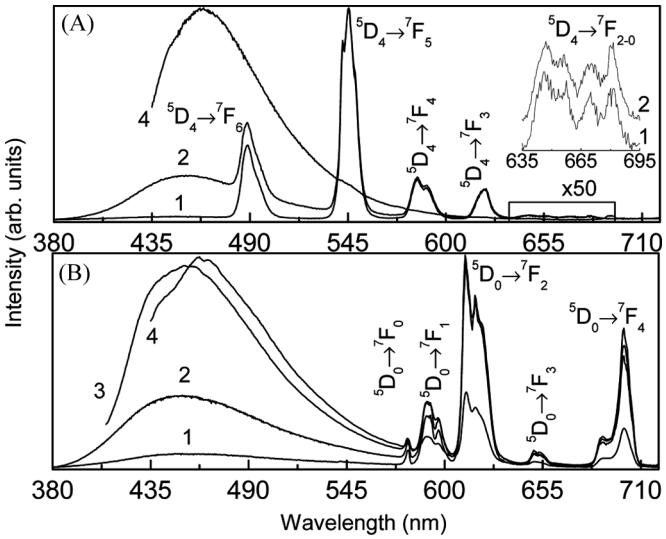

FIGURE 5 **Room temperature emission spectra of (A) M-Eu and (B) M-Tb excited at 1) 270, 2) 360, 3) 393 and 4) 420 nm. The inset shows a magnification of the $^5D_4 \rightarrow {}^7F_{2-0}$ transitions; the spectra were dislocated along the y-axis to render easier the visualization.**

wavelength. In particular, for excitation wavelengths between 270 and 360 nm the broad band energy remains essentially unaltered, peaking at *ca.* 450 nm. The increase of the excitation wavelength (360 to 460 nm) leads to the decrease of the emission energy. A similar broad band displaying an analogous dependence on the excitation wavelength was already observed in the non-doped **M** host (Fig. 6) and in a urea-bpy bridged silsesquioxane derived from the same precursor under different nucleophilic conditions.[21] Time-resolved experiments demonstrated that this emission is ascribed to a superposition of three distinct components: i) bpy triplet state (at *ca.* 450 nm, room temperature lifetime of 10^{-5}–10^{-4} s); electron-hole recombinations originated in the ii) NH/C=O groups of the urea cross-linkages (*ca.* 530 nm) and iii) siliceous nanoclusters (*ca.* 427 nm). These two latter components (with a room temperature lifetime value of 10^{-9} s) were also observed in analogous organic/inorganic hybrids.[22–24]

Figure 7 shows the excitation spectra of **M-Eu** and **M-Tb** monitored within the Eu^{3+} $^5D_0 \rightarrow {}^7F_2$ and Tb^{3+} $^5D_4 \rightarrow {}^7F_5$ transitions, respectively. The spectra are composed of a broad band with two main components (260 to 280 nm and 320 to 340 nm) overlapped with the intra-$4f^6$ $^7F_0 \rightarrow {}^5L_6, {}^5D_2$, $^7F_{0,1} \rightarrow {}^5D_1$ and intra-$4f^8$ $^7F_6 \rightarrow {}^5D_4$ transitions, for **M-Eu** and **M-Tb**, respectively. A low-relative intensity band between 360 and 450 nm (more evident in the excitation spectrum of **M-Eu**) is also discerned. While the low-wavelength region (240 to 360 nm) is related to the excited states of the bpy-ligands,[14,21,25] the high-wavelength one (360 to 450 nm) is associated with the excited states of the NH/C=O groups and of the siliceous nanoclusters,[22–24] as shown in the excitation spectra monitored within the hybrid emission (Fig. 7). The presence of either the bpy and hybrid host excited states in the excitation spectra monitored within the Eu^{3+} and Tb^{3+} excited states points out the presence of bpy/hybrid-to-Ln^{3+} energy transfer. Moreover, the negligible relative intensity of the intra-4f lines, points out that

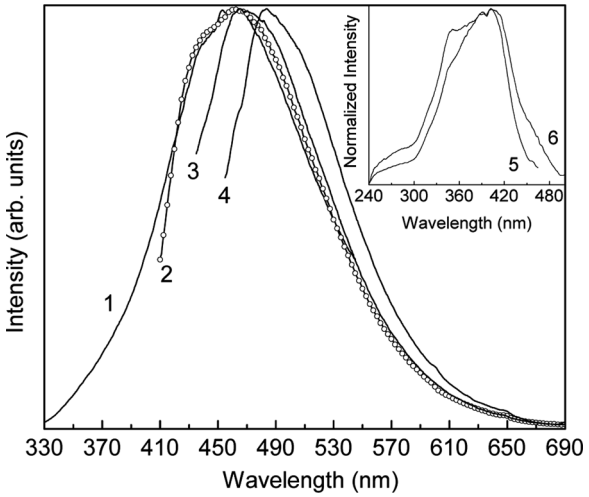

FIGURE 6 **Room temperature emission spectra of M excited at 1) 280, 2) 395, 3) 420 and 4) 440 nm. The inset shows the excitation spectra monitored at 5) 480 and 6) 540 nm.**

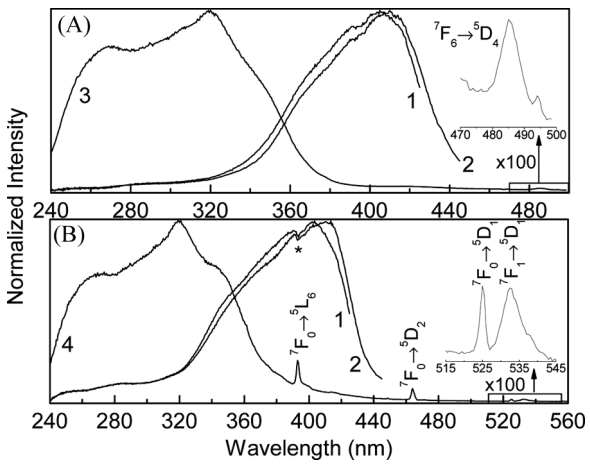

FIGURE 7 **Room temperature excitation spectra of (A) M-Eu and (B) M-Tb monitored at 1) 440, 2) 460, 3) 544 and 4) 612 nm. The asterisk denotes the $^7F_0 \rightarrow {}^5L_6$ self-absorption. The insets show a magnification of the $^7F_6 \rightarrow {}^5D_4$ (A) and $^7F_{0,1} \rightarrow {}^5D_1$ transitions.**

the Ln^{3+} ions sensitization is more efficient than direct intra-4f excitation.

The lifetime (τ) values of the Eu^{3+} and Tb^{3+} excited states ($^5D_0$ and $^5D_4$, respectively) were monitored at 700 and 544 nm and excited at 464 and 330 nm, respectively, at 11 and 300 K. All the emission decay curves are well reproduced by a single exponential function yielding $\tau(^5D_0) = 0.456 \pm 0.005 \times 10^{-3}$ s and $\tau(^5D_4) = 0.913 \pm 0.004 \times 10^{-3}$ s, at 14 K, and $\tau(^5D_0) = 0.384 \pm 0.016 \times 10^{-3}$ s and $\tau(^5D_4) = 0.868 \pm 0.007 \times 10^{-3}$ s, at 300 K.

Figure 8 shows the room temperature emission spectra of **M-EuTb** which is strongly dependent on the excitation wavelength. For excitation wavelengths between 270 and 340 nm, the emission features are essentially attributed to the overlap of the Eu^{3+} and Tb^{3+} $^5D_0 \rightarrow {}^7F_{0-4}$ and the $^5D_4 \rightarrow {}^7F_{6,5}$ transitions, respectively. At higher excitation wavelengths (340 to 393 nm), besides the intra-4f transitions the above mentioned hybrid's host emission is observed.

Accordingly, the emission colour is fine-tuned across the *Commission Internationale d'Éclairage* (CIE) chromaticity diagram (Fig. 9) from the red (**M-Eu**), orange (**M-EuTb**) or green (**M-Tb**) regions to the blue one, by changing the excitation wavelength. Interestingly, upon excitation at 360 nm, the (x,y) color coordinates of **M-EuTb** (0.32,0.29) get close to the white point (0.33,0.33) making it white light emitter.

The excitation spectra were selectively monitored within the Eu^{3+} and Tb^{3+} $^5D_0 \rightarrow {}^7F_4$ (700 nm) and $^5D_4 \rightarrow {}^7F_5$ (544 nm) transitions, respectively (Fig. 10). Both spectra are similar, consisting of a large broad band with two main components peaking at 270 and 340 nm and of a shoulder at 410 nm, resembling the spectrum acquired for **M** (inset in Fig. 6) and for **M-Ln** (Fig. 5). Therefore, the high- and low-wavelength regions can be attributed to the preferential excitation of the bpy and NH/C=O groups and siliceous nanoclusters, respectively. The spectrum

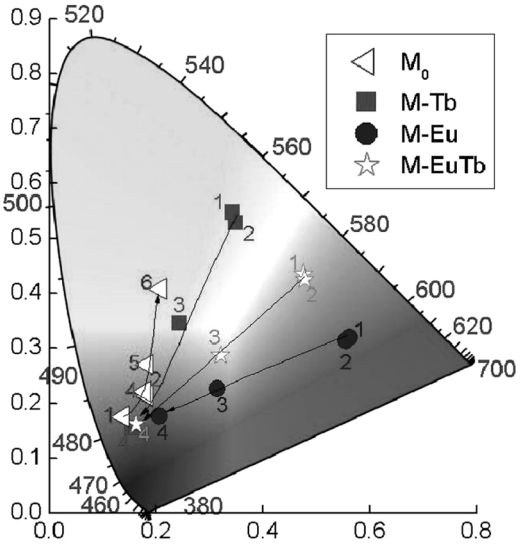

FIGURE 9 **Chromaticity diagram (CIE, 1931) showing the (x,y) emission color coordinates of M, M-Eu, M-Tb, and M-EuTb under different excitation wavelengths. The arrow indicates the excitation wavelength variation: (1) 270, (2) 320, (3) 360, (4) 400, (5) 420, and (6) 440 nm.**

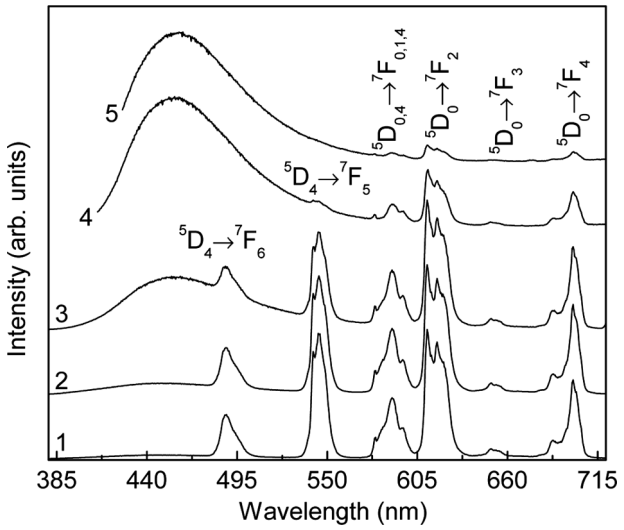

FIGURE 8 **Room temperature emission spectra of M-EuTb excited at 1) 270, 2) 340, 3) 364, 4) 393 and 5) 410 nm.**

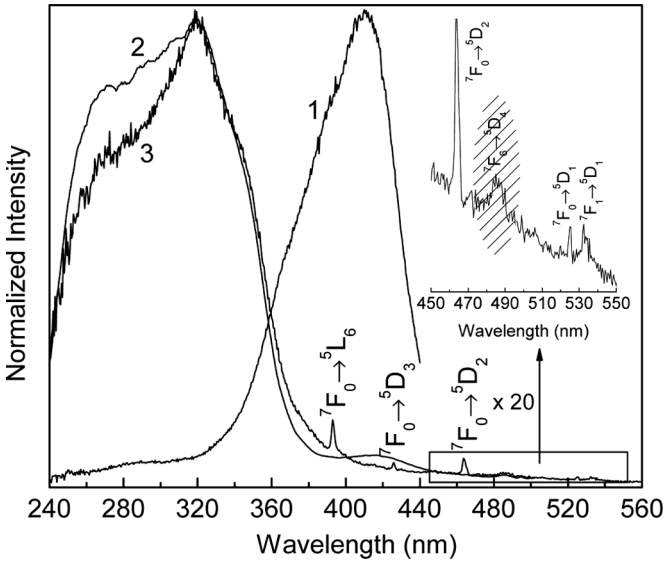

FIGURE 10 **Room temperature excitation spectra of M-EuTb monitored at 1) 460, 2) 544 and 3) 700 nm. The inset shows a magnification of the spectrum monitoring the Eu^{3+} emission at 700 nm.**

selectively monitored within the Eu^{3+} lines displays low relative intensity intra-4f transitions ($^7F_0 \rightarrow {}^5L_6, {}^5D_{3-1}$, $^7F_1 \rightarrow {}^5D_1$, Eu^{3+}, and $^7F_6 \rightarrow {}^5D_4$, Tb^{3+}). The observation of the Tb^{3+}-related transition is a clear evidence of the occurrence of Tb^{3+}-to-Eu^{3+} energy transfer at room temperature. The spectra acquired at 11 K (not shown) are similar to those measured at room temperature. The $^5D_0$ and $^5D_4$ decay curves are non-exponential (Fig. 11 of Supporting Information) illustrating the multiple and complex energy transfer scheme (bpy → hybrid → $Tb^{3+} \rightarrow Eu^{3+}$, bpy → hybrid → Ln^{3+} and hybrid → Ln^{3+}) of **M-EuTb**. The analysis of these mechanisms lies outside the scope of the present work.

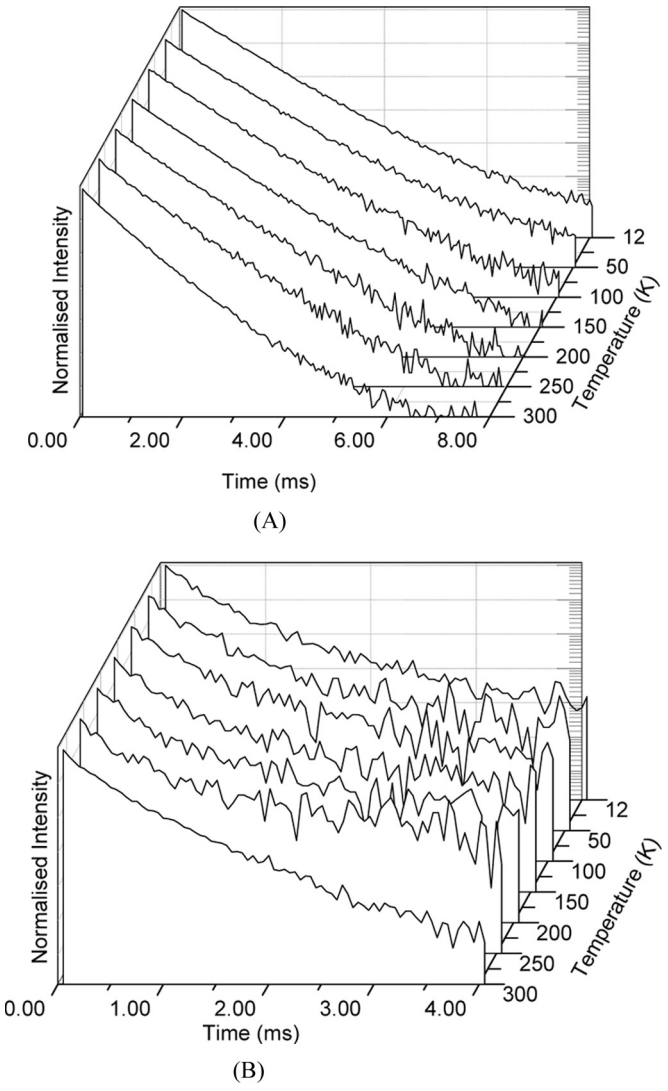

FIGURE 11 **Selected emission decay curves of M-EuTb acquired in the temperature range of 12 to 300 K (A) monitored at 544 nm and excited at 330 nm and (B) monitored at 700 nm and excited at 465 nm.**

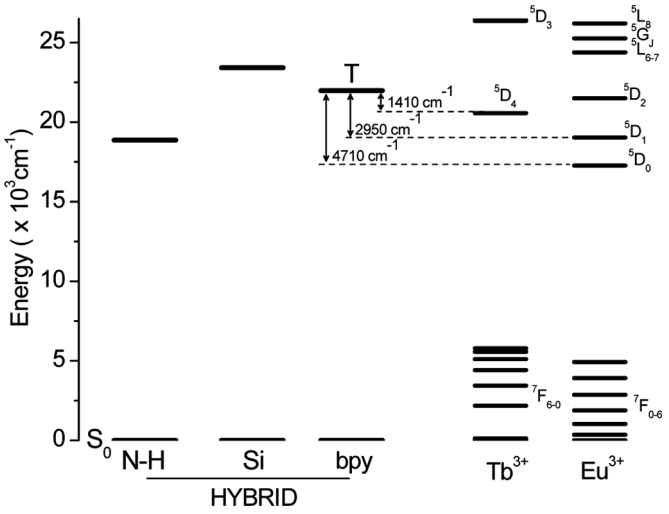

FIGURE 12 **Schematic illustration of the partial energy diagram level showing the Tb^{3+} and Eu^{3+} intra-4f levels and the energy peak position of the hybrid host emitting centers, urea-(N-H), siliceous-related (Si) components and bpy-triplet state. For the sake of clarity, the first excited Gd^{3+} level ($^6P_{7/2}$) at *ca.* 32.000 cm^{-1} is omitted.**

The energy levels of the hybrid host emitting centres (Fig. 12) were determined from the emission spectra of **M-Gd** (Fig. 13), since Gd^{3+} excited levels have energies much higher than those of the hybrid host excited states, thus disabling host-to-Ln^{3+} energy transfer. A fitting procedure assuming a sum of multi-Gaussian functions was used (Fig. 13). The emission

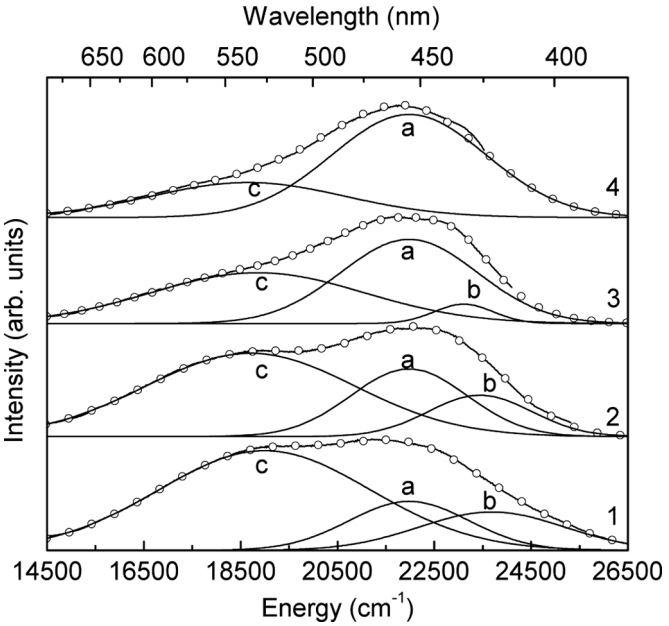

FIGURE 13 **Emission spectra (11 K) of M-Gd excited at 1) 360, 2) 380, 3) 400, and 4) 420 nm. The fit components are also presented: a) bpy-triplet state, electron-hole recombinations occurring in the b) siliceous domains, and c) urea cross-linkages. The open circles represent the fit envelope.**

spectra excited at 420 nm is well modelled by a sum of two Gaussian functions peaking at 530 nm (18867 cm^{-1}) and 455 nm (21978 cm^{-1}) ascribed, respectively, to the NH-related emission[22–24] and to the triplet state of the bpy,[21] At lower excitation wavelengths a third Gaussian component, whose peak position deviates towards the red as the excitation wavelength increases, is discerned and can be attributed to the siliceous nanodomains.[22–24] Owing to the emission dependence on the excitation wavelength an average peak position at 427 nm (24414 cm^{-1}) was used in the diagram of Fig. 12.

The detection of a single $^5D_0 \rightarrow {}^7F_0$ line, the J-degeneracy splitting of the $^7F_{1,2}$ levels into 3 and 4 Stark components, respectively, indicate that the Eu^{3+} ions in **M-Eu** and **M-TbEu** occupy the same average local environment with a low symmetry site, without an inversion center, in accordance with the higher intensity of the electric-dipole $^5D_0 \rightarrow {}^7F_2$ transition.[26] The energy and fwhm of the $^5D_0 \rightarrow {}^7F_0$ line were estimated using a single Gaussian fit, yielding to $17270.8 \pm 0.4\,cm^{-1}$ and $41.6 \pm 0.9\,cm^{-1}$, for **M-Eu**, and $17263.2 \pm 0.5\,cm^{-1}$ and $50.4 \pm 1.5\,cm^{-1}$, for **M-EuTb**. The higher energy of the $^5D_0 \rightarrow {}^7F_0$ transition found for the former hybrid indicates that the Eu-ligand bonds have (on average) a less covalent character relative to the situation found in the latter.[1,26–29] This observation suggests variations in the number and/or type of Eu^{3+}-first neighbours (as it will be further discussed below), which could be caused by the different relative Eu^{3+} content in **M-Eu** and **M-EuTb** (4.98 and 2.68% w/w, respectively). Moreover, the large values found for the fwhm (higher than those reported for analogous amorphous hybrids, 19 to 37 cm^{-1}),[21,30] point out that the Eu^{3+} cations are accommodated in a continuous distribution of similar local sites.

From the emission spectra shown in Fig. 14 we have determined the experimental intensity parameters, Ω_2 and Ω_4, of **M-Eu** and **M-EuTb** by using the $^5D_0 \rightarrow {}^7F_2$ and $^5D_0 \rightarrow {}^7F_4$ electronic transitions, respectively, and by expressing the emission intensity (I) in terms of the surface (S) under the emission curve as:

$$I_{i\rightarrow j} = \hbar w_{i\rightarrow j} A_{i\rightarrow j} N_i \equiv S_{i\rightarrow j} \qquad (1)$$

where i and j represent the initial ($^5D_0$) and final ($^7F_{0\text{-}4}$) levels, respectively, $\hbar\omega_{i\rightarrow j}$ is the transition

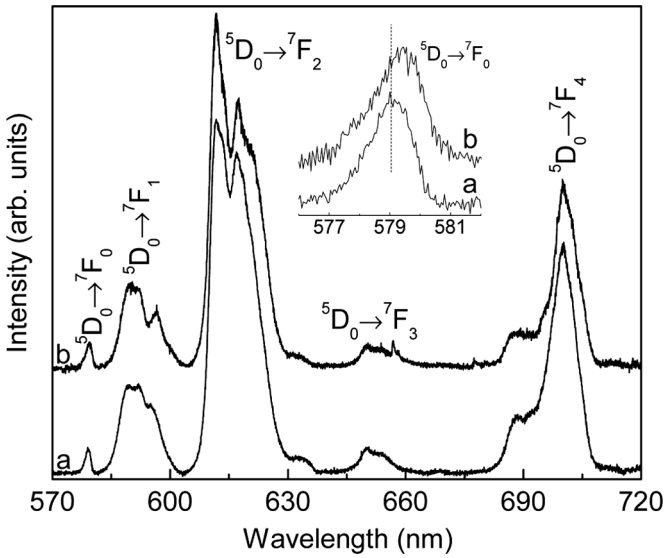

FIGURE 14 **Room temperature high resolution emission spectra excited at 464 nm of a) M-Eu and b) M-EuTb. The inset shows a magnification of the $^5D_0 \rightarrow {}^7F_0$ transitions.**

energy, $A_{i\rightarrow j}$ corresponds to Einstein's coefficient of spontaneous emission and N_i is the population of the $^5D_0$ emitting level. The magnetic dipole allowed $^5D_0 \rightarrow {}^7F_1$ transition may be taken as the reference and, hence, the total radiative rate is expressed by:[1,31,32]

$$A_r = \sum_{J=0}^{4} A_{0J} = \frac{A_{01}\hbar\varpi_{01}}{S_{01}} \times \sum_{J=0}^{4} \frac{S_{0J}}{\hbar\varpi_{0J}}. \qquad (2)$$

The total radiative emission rate A_r could be also expressed in terms of the intensity parameters as:[1,27,33]

$$A_r = \frac{4e^2\omega^3}{3\hbar c^3}\chi \sum_{\lambda} \Omega_\lambda \left\langle {}^7F_J \| U^{(\lambda)} \| {}^5D_0 \right\rangle^2 \frac{1}{2J+1} \qquad (3)$$

where $\lambda = 2$ and 4, χ is the Lorentz local-field correction term that is given by $n(n^2+2)^2/9$ (a refraction index $n = 1.5$ is considered) and $\langle {}^7F_J \| U^{(\lambda)} \| {}^5D_0 \rangle$ are the squared reduced matrix elements whose values are 0.0032 and 0.0023 for $J = 2$ and 4, respectively.[1,11,33] The Ω_6 parameter was not determined, since the $^5D_0 \rightarrow {}^7F_{5,6}$ transitions are not observed experimentally. The values of the Ω_2 and Ω_4 experimental intensity parameters are, respectively, 6.7×10^{-20} and $4.3 \times 10^{-20}\,cm^2$, for **M-Eu**, and 7.9×10^{-20} and $5.1 \times 10^{-20}\,cm^2$, for **M-EuTb**. The

relative high values of Ω_2 might be interpreted as a consequence of the hypersensitive behavior of the $^5D_0 \rightarrow {}^7F_2$ transition, suggesting that the dynamic coupling mechanism is quite operative and that the chemical environment is highly polarizable. In particular, a correlation has been noticed in the sense that compounds expected to have a higher degree of covalence tend to present higher values of Ω_2.[10,27,32,33] The Ω_2 values estimated for **M-Eu** are smaller than those calculated for **M-EuTb**, pointing out a decrease in the average degree of covalence of the Eu-first bonds in **M-Eu**, in agreement with the above mentioned conclusions derived from the analysis of the energy of the $^5D_0 \rightarrow {}^7F_0$ transition the in the two hybrids. Furthermore, the Ω_2 values are similar to those previously found for amorphous amine-functionalised organic/inorganic hybrids incorporating europium triflate salt,[1,27] for analogous lamellar hybrids incorporating $EuCl_3$[1,11] and mesostructured silica doped with aquo-Eu^{3+} β-diketonate complex,[1,34] despite the distinct morphologies and Eu^{3+}-local coordination sites found in all these hybrids. It is also interesting to note that in these hybrids (except for the mesostructured silica-based hybrid) and in **M-Eu** and **M-EuTb** the Ω_2 and Ω_4 values are of the same order of magnitude, regardless of the fact that in a larger number of Eu^{3+}-containing hybrids the Ω_4 values are substantially smaller than those of Ω_2.[1]

The non-radiative rate A_{nr} of **M-Eu** was obtained from the calculated A_r rate and the experimental $^5D_0$ decay time by using the relation:

$$\tau^{-1} = A_T = A_r + A_{nr}. \quad (4)$$

The $^5D_0$ quantum efficiency (η) was evaluated from the ratio between A_r and A_T, $\eta = \frac{A_r}{A_r + A_{nr}}$, yielding $A_r = 362\,s^{-1}$, $A_{nr} = 2245\,s^{-1}$ and $\eta = 0.14$. The A_{nr} value may be rationalised in terms of the number of water molecules coordinated to Eu^{3+} (n_w) as determined from the empirical formula:[35]

$$n_w = 1.11 \times (A_T - A_r - 0.31). \quad (5)$$

For **M-Eu** $n_w = 2.1 \pm 0.1$. We note that similarly to the situation found for the intensity parameters, the η and n_w values estimated for **M-Eu** are very close to those reported for the above mentioned di-ureasils,[1,27] **L12**[1,11] and SBA-15[1,34] Eu^{3+}-based hybrids.

The emission absolute quantum yield was measured for all the hybrids. For the non-doped **M** a maximum value of 0.18 ± 0.02 was reached under excitation in the long-wavelength UV and blue spectral regions (360 to 420 nm). The most efficient organic-inorganic hybrid lacking activator metal ions reported is 3-aminopropyltriethoxysilane (APTES)-formic acid hybrid with a quantum yield value of 0.35 ± 0.1 under UV excitation (360 nm).[36] We should stress that despite the lower quantum yield value measured for **M** (0.18 ± 0.02) it is obtained under long UV/blue excitation. Moreover, this is the second higher quantum value measured under this excitation range below that recently reported for an analogous urea-bpy bridged silsesquioxane derived from the same precursor under different nucleophilic conditions.[21]

For the Eu^{3+}- and Tb^{3+}-containing hybrids the maximum quantum yield values were attained under excitation *via* the bpy-triplet (320 nm), 0.08 (**M-Eu**) and 0.12 (**M-Tb** and **M-EuTb**). The higher quantum yield values obtained for the Tb^{3+}-containing hybrids can be accounted for the higher resonance between the bpy-triplet state with the $^5D_4$ level of Tb^{3+} ions ($1410\,cm^{-1}$), relatively to that found for the $^5D_1$ level of Eu^{3+} ions ($2950\,cm^{-1}$), Fig. 13. Under excitation via the urea cross-linkages and siliceous domains excited states (380 to 420 nm) the quantum yield values are lower, independently of the selected excitation wavelength, 0.06 (**M-Eu**) and 0.08 (**M-Tb** and **M-EuTb**), pointing out the active role of bpy in the enhancement of the emission quantum yield values of Ln^{3+}-based hybrids.

CONCLUSIONS

Urea-based bis-silylated bpy organic–inorganic hybrids incorporating different lanthanides ions (Eu^{3+}, Gd^{3+} and Tb^{3+}, ca. 5–7% w/w) were obtained by the sol–gel process. The hybrids are room temperature multi-wavelength emitters due to the convolution of the emission arising from the hybrid's emitting centers (urea cross-linkages, siliceous domains and bpy triplet) and the Eu^{3+} and/or Tb^{3+} intra-4f transitions. The emission color is easily tuned across the CIE diagram from the blue to the red, orange or green areas, depending on the Ln^{3+} ions and the excitation wavelength. Bpy-to-Ln^{3+} and Tb^{3+}-to-Eu^{3+} energy transfer mechanisms are

demonstrated in the different hybrids. Due to the different bpy/Ln^{3+} ratios, the Eu^{3+}-local coordination in the Eu^{3+} and Eu^{3+}/Tb^{3+} co-doped samples slightly differ, as shown by the $^5D_0 \rightarrow {}^7F_{0-4}$ transition energies, $^5D_0$ lifetimes and intensity parameters. Although it could not be determined precisely, the Ln^{3+} coordination sphere was shown to comprise bpy fragments, chloride anions and water molecules (1 to 2). Improvement of the hybrids' performances through the control of the organic fragments will potentially allow applications as layers for active photonic devices. Work is underway along these lines.

REFERENCES

1. Carlos, L. D.; Ferreira, R. A. S.; de Zea Bermudez, V.; Ribeiro, S. J. L. Lanthanide-containing light-emitting organic-inorganic hybrids: A bet on the future. *Adv. Mater.* **2009**, *21*, 509–534.
2. Binnemans, K. Lanthanide-based luminescent hybrid materials. *Chem. Rev.* **2009**, *109*, 4283–4374.
3. Escribano, P.; Julian-Lopez, B.; Planelles-Arago, J.; Cordoncillo, E.; Viana, B.; Sanchez, C. Photonic and nanobiophotonic properties of luminescent lanthanide-doped hybrid organic-inorganic materials. *J. Mater. Chem.* **2008**, *18*, 23–40.
4. Kaes, C.; Katz, A.; Hosseini, M. W. Bipyridine: The most widely used ligand. A review of molecules comprising at least two 2,2′-bipyridine units. *Chem. Rev.* **2000**, *100*, 3553–3590.
5. Puntus, L. N.; Lyssenko, K. A.; Pekareva, I. S.; Bunzli, J. C. G. Intermolecular interactions as actors in energy-transfer processes in lanthanide complexes with 2,2′-Bipyridine. *J. Phys. Chem. B* **2009**, *113*, 9265–9277.
6. Franville, A. C.; Zambon, D.; Mahiou, R.; Troin, Y. Luminescence behavior of sol-gel-derived hybrid materials resulting from covalent grafting of a chromophore unit to different organically modified alkoxysilanes. *Chem. Mater.* **2000**, *12*, 428–435.
7. Li, H. R.; Lin, J.; Zhang, H. J.; Li, H. C.; Fu, L. S.; Meng, Q. G. Novel, covalently bonded hybrid materials of europium (terbium) complexes with silica. *Chem. Commun.* **2001**, *13*, 1212–1213.
8. Li, H.; Yu, J.; Liu, F.; Zhang, H.; Fu, L.; Meng, Q.; Peng, C.; Lin, J. Preparation and luminescence properties of in situ formed lanthanide complexes covalently grafted to a silica network. *New J. Chem.* **2004**, *28*, 1137–1141.
9. Cousinié, S.; Gressier, M.; Alphonse, P.; Menu, M. J. Silica-based nanohybrids containing dipyridine, urethan, or urea derivatives. *Chem. Mater.* **2007**, *19*, 6492–6503.
10. Li, H.; Lin, N.; Wang, Y.; Feng, Y.; Gan, Q.; Zhang, H.; Dong, Q.; Chen, Y. Construction and photoluminescence of monophase hybrid materials derived from a urea-based bis-silylated bipyridine. *Eur. J. Inorg. Chem.* **2009**, *4*, 519–523.
11. Nobre, S. S.; Brites, C. D. S.; Ferreira, R. A. S.; de Zea Bermudez, V.; Carcel, C.; Moreau, J. J. E.; Rocha, J.; Wong Chi Man, M.; Carlos, L. D. Photoluminescence of Eu(III)-doped lamellar bridged silsesquioxanes self-templated through a hydrogen bonding array. *J. Mater. Chem.* **2008**, *18*, 4172–4182.
12. Benyahya, S.; Monnier, F.; Taillefer, M.; Wong Chi Man, M.; Bied, C.; Ouazzani, F. Efficient and versatile sol-gel immobilized copper catalyst for ullmann arylation of phenols. *Adv. Synth. Cat.* **2008**, *350*, 2205–2208.
13. Fu, L. S.; Ferreira, R. A. S.; Silva, N. J. O.; Carlos, L. D.; de Zea Bermudez, V.; Rocha, J. Photoluminescence and quantum yields of urea and urethane cross-linked nanohybrids derived from carboxylic acid solvolysis. *Chem. Mater.* **2004**, *16*, 1507–1516.
14. Tsaryuk, V.; Zolin, V.; Legendziewicz, J.; Szostak, R.; Gawryszewska, P. Optical spectroscopy of europium nitrate with 2,2′-bipyridine $Eu(NO_3)_3 \cdot Bpy_3$. One more of compounds with outer-sphere Bpy molecule? *J. Alloy Compd.* **2004**, *380*, 418–425.
15. Qin, J. G.; Yang, C. L.; Yakushi, K.; Nakazawa, Y.; Ichimura, K. Synthesis and properties of a new ferromagnetic 2,2′-bipyridine-$MnPS_3$ intercalation compound. *Solid State Commum.* **1996**, *100*, 427–431.
16. Preda, N.; Mihut, L.; Baibarac, M.; Baltog, I.; Husanu, M.; Bucur, C.; Velula, T. The Intercalation of PbI_2 with 2,2-bipyridine evidenced by photoluminescence, FT-IR and raman spectroscopy. *Rom. J. Phys.* **2008**, *54*, 667–675.
17. Pozat, Q.; Sourisseau, C. Infrared, raman, and resonance raman studies of the $Ru(2,2'\text{-bpy})_3^{2+}$ cation in its chloride crystal and as an Intercalate in the Layered $MnPS_3$ compound. *J. Phys. Chem.* **1984**, *88*, 3007–3014.
18. Álvaro, M.; Fornés, V.; García, S.; García, H.; Scaiano, J. C. Intrazeolite photochemistry. 20. Characterization of highly luminescent europium complexes inside zeolites. *J. Phys. Chem. B* **1998**, *102*, 8744–8750.
19. Minaev, B. F.; Minaeva, V. A.; Baryshnikov, G. V.; Girtu, M. A.; Agren, H. Theoretical study of vibration spectra of sensitizing dyes for photoelectrical converters based on ruthenium(II) and iridium(III) complexes. *Russ. J. Appl. Chem.* **2009**, *82*, 1211–1221.
20. Soptrajanov, B.; Trpkosvska, M.; Pejov, L. Fourier transform infrared study of dichlorodioxochromium(VI), dichlorodioxomolybdenum(VI) and dichlorodioxotungsten(VI) complexes with 2,2′-bipyridine. *Croatica Chem. Acta* **1999**, *72*, 663–672.
21. Nobre, S. S.; Cattoën, X.; Ferreira, R. A. S.; Wong Chi Man, M.; Carlos, L. D. Efficient spectrally dynamic blue–to–green emission of bipyridine–based bridge silsequioxanes for solid–state lighting. *Phys. Status Solidi RRL*. **2010**, *4*, 55–57.
22. Carlos, L. D.; Ferreira, R. A. S.; de Zea Bermudez, V.; Ribeiro, S. J. L. Full-color phosphors from amine-functionalized crosslinked hybrids lacking metal activator ions. *Adv. Funct. Mater.* **2001**, *11*, 111–115.
23. Carlos, L. D.; Ferreira, R. A. S.; Pereira, R. N.; Assunção, M.; de Zea Bermudez, V. White-light emission of amine-functionalized organic/inorganic hybrids: Emitting centers and recombination mechanisms. *J. Phys. Chem. B* **2004**, *108*, 14924–14932.
24. Nobre, S. S.; Lima, P. P.; Mafra, L.; Ferreira, R. A. S.; Freire, R. O.; Fu, L. S.; Pischel, U.; de Zea Bermudez, V.; Malta, O. L.; Carlos, L. D. Energy transfer and emission quantum yields of organic-inorganic hybrids lacking metal activator centers. *J. Phys. Chem. C.* **2007**, *111*, 3275–3284.
25. Song, X. Q.; Zheng, H. R.; Liu, W. S.; Ju, Z. H. Synthesis, structure and spectroscopic properties of rare earth complexes with a new aryl amide 2,2′-bipydine derivative. *Spectrochimica Acta Part A* **2008**, *69*, 49–55.
26. Carlos, L. D.; Ferreira, R. A. S.; de Zea Bermudez, V.; Molina, C.; Bueno, L. A.; Ribeiro, S. J. L. White light emission of Eu^{3+}-based hybrid xerogels. *Phys. Rev. B* **1999**, *60*, 10042–10053.
27. Carlos, L. D.; Messaddeq, Y.; Brito, H. F.; Ferreira, R. A. S.; de Zea Bermudez, V.; Ribeiro, S. J. L. Full-color phosphors from europium(III)-based organosilicates. *Adv. Mater.* **2000**, *12*, 594–598.
28. Malta, O. L.; Batista, H. J.; Carlos, L. D. Overlap polarizability of a chemical bond: a scale of covalency and application to lanthanide compounds. *Chem. Phys.* **2002**, *282*, 21–30.
29. Carlos, L. D.; Malta, O. L.; Albuquerque, R. Q. A covalent fraction model for lanthanide compounds. *Chem. Phys. Lett.* **2005**, *416*, 238–242.
30. Fu, L. S.; Ferreira, R. A. S.; Silva, N. J. O.; Fernandes, J. A.; Ribeiro-Claro, P.; Goncalves, I. S.; de Zea Bermudez, V.; Carlos, L. D. Structure-photoluminescence relationship in Eu(III) beta-diketonate-based organic-inorganic hybrids. Influence of the synthesis method: Carboxylic acid solvolysis versus conventional hydrolysis. *J. Mater. Chem.* **2005**, *15*, 3117–3125.
31. Malta, O. L.; Coutos dos Santos, M. A.; Thompson, L. C.; Ito, N. K. Intensity parameters of 4f-4f transitions in the Eu(dipivaloylmethanate)(3) 1,10-phenanthroline complex. *J. Lumin.* **1996**, *69*, 77–84.

32. Malta, O. L. Ligand-rare-earth ion energy transfer in coordination compounds. A theoretical approach. *J. Lumin.* **1997**, *71*, 229–236.
33. Lima, P. P.; Ferreira, R. A. S.; Freire, R. O.; Paz, F. A. A.; Fu, L. S.; Alves, S.; Carlos, L. D.; Malta, O. L. Spectroscopic study of a UV-photostable organic-inorganic hybrids incorporating an Eu^{3+} beta-diketonate complex. *Chemphyschem* **2006**, *7*, 735–746.
34. Peng, C. Y.; Zhang, H. J.; Yu, J. B.; Meng, Q. G.; Fu, L. S.; Li, H. R.; Sun, L. N.; Guo, X. M. Synthesis, characterization, and luminescence properties of the ternary europium complex covalently bonded to mesoporous SBA-15. *J. Phys. Chem. B* **2005**, *109*, 15278–15287.
35. Supkowski, R. M.; Horrocks, W. D. On the determination of the number of water molecules, q, coordinated to europium(III) ions in solution from luminescence decay lifetimes. *Inorg. Chim. Acta* **2002**, *340*, 44–48.
36. Green, W. H.; Le, K. P.; Grey, J.; Au, T. T.; Sailor, M. J. White phosphors from a silicate-carboxylate sol-gel precursor that lack metal activator ions. *Science* **1997**, *276*, 1826–1828.